Dynamic Molecular Structure of Plant Biomass-derived Black Carbon (Biochar)

Marco Keiluweit [†], Peter S. Nico[‡], Mark G. Johnson[§], and Markus Kleber[†,*]

Department of Crop and Soil Science, Oregon State University

University of California - Berkeley, Lawrence Berkeley National Laboratory, Earth Sciences Division

U.S. Environmental Protection Agency, National Health and Environmental Effects Research Laboratory, Corvallis

[†] Oregon State University

[‡] Lawrence Berkeley National Laboratory

[§] U.S. Environmental Protection Agency

*corresponding author phone: (01)-541-737-5718; email: markus.kleber@oregonstate.edu

Abstract

Char black carbon (BC), the solid residue of incomplete combustion, is continuously being added to soils and sediments due to natural vegetation fires, anthropogenic pollution, and new strategies for carbon sequestration ('biochar'). Here we present a molecular-level assessment of the physical organization and chemical complexity of biomass-derived chars and, specifically, that of aromatic carbon in char structures. BET-N_2 surface area, X-ray diffraction (XRD), synchrotron-based Near-edge X-ray Absorption Fine Structure (NEXAFS), and Fourier transform infrared (FT-IR) spectroscopy are used to show how two plant materials (wood and grass) undergo analogous, but quantitatively different physical-chemical transitions as charring temperature increases from 100 to 700˚C. These changes suggest the existence of four distinct categories of char consisting of a unique mixture of chemical phases and physical states: (i) in transition chars the crystalline character of the precursor materials is preserved, (ii) in amorphous chars the heat-altered molecules and incipient aromatic polycondensates are randomly mixed, (iii) composite chars consist of poorly ordered graphene stacks embedded in amorphous phases, and (iv) turbostratic chars are dominated by disordered graphitic crystallites. The molecular variations among the different char categories translate into differences in their ability to persist in the environment and function as environmental sorbents.

Introduction

Black carbon (BC) is an important constituent of soils and sediments (*1-4*). BC has received much attention for three reasons. First, there is a general lack of knowledge of the processes that lead to the loss of BC from soils and sediments which prevents a clear understanding of fluxes into and out of the Earth's slow cycling C pools (*3*). Second, the addition of synthetic BC ("biochar") in soils combined with bioenergy production has been suggested as a means to mitigate climate change (*5, 6*). Finally, BC in soils and sediments is recognized as an effective sorbent for potentially hazardous organic compounds (*2, 7*). Evidently, there is gathering interest in understanding the behavior of BC; precise information regarding the structure and properties of BC is needed. However, BC is not a well-defined chemical substance and encompasses C forms with varying degrees of aromaticity such as partly charred plant matter, char, soot, and graphite (*8*). This fact creates difficulties in quantifying BC concentrations in natural environments (*9*), it complicates the identification of biochars with properties beneficial to soils (*5*), and results in large variations in the sorptive potential of BC (*10*). Masiello (*3*) summarized the nature of the problem when she stated: "discrepancies between BC studies occur at least in part because of a lack of a common model of BC."

Biomass-derived char BC is defined as the solid residue of incomplete combustion. A widely accepted conceptual approach to represent the transient chemical properties of char BC is based on the gradual increase in aromaticity observed for the heat-induced transformation of plant biomass into char (*3, 11*). This concept is commonly referred to as the "combustion continuum" and assumes that, with increasing charring temperature, plant biomass undergoes chemical transformations leading to the formation of aromatic ring structures, followed by a progressive condensation of smaller aromatic units into larger conjugated sheets (*4*). Recently,

Knicker and co-workers (*12*, *13*) conceptualized char BC created at a temperature of 350˚C and in the presence of O_2 as a heterogeneous mixture of thermally altered biomacromolecules with substantial substitution with O, H, and S and average cluster sizes of aromatic units smaller than six rings.

While Knicker et al. did not attempt to relate physical properties of their char BC to its molecular structure, the recent past has revealed indications of the occurrence of nonlinearities and phase transitions during the thermal decomposition of biomass, which can be explained only by relatively abrupt changes in physical properties of chars, namely crystallinity and porosity. For instance, N_2-accessible surface area (SA) of char BC exhibits a rapid increase at intermediate charring temperatures (*5*, *10*). This is approximately the same temperature region where X-ray diffraction data (*14-16*) show a transition from low-density disordered C to the formation of turbostratic crystallites.

It thus appears critical for the prediction of fate and reactivity of char BC to relate the evolution of the chemical structure of chars created across a relevant temperature range to their physical properties. Consequently, the primary objective of this study is to integrate physical and chemical information into a comprehensive model for the physical nature of plant biomass-derived char. We test the hypothesis that physical transitions expressed by changes in SA along a representative charring temperature range are reflected in corresponding changes in crystal structure as determined by X-ray diffraction. We further explore the extent to which physical phase transitions as observed by Paris et al. (*16*) are reflected in chemical changes, and test whether this information can be combined with chemical data to recognize specific categories of chars.

Plant biomass variability is considered by using lignin-rich Pine wood shavings (*Pinus ponderosa*) and lignin poor Tall fescue grass (*Festuca arundinacea*) starting materials for char production across a charring temperature range of 100 to 700˚C. The properties of the chars are characterized via elemental and gravimetric analysis, BET-N_2 SA measurements, and Fourier transform infrared spectroscopy. Synchrotron-based near-edge X-ray absorption fine structure spectroscopy at the carbon K absorption edge is employed to relate C speciation to the degree of structural order of carbonaceous matter.

Experimental Section

Production. Commercially available Ponderosa Pine shavings were purchased through GEM Shavings in Auburn, WA. Tall Fescue straw was collected at the Oregon State University Hyslop Field Research Laboratory in Corvallis, OR. After grinding to obtain a particle size of less than 1.5 mm, the materials were charred at 100, 200, 300, 400, 500, 600 and 700˚C for 1 hour in a closed container under oxygen-limited conditions in a 550 Series Fisher Scientific Isotemp muffle furnace (Fisher Scientific, Pittsburgh, PA). Char yield was recorded and the samples were milled to pass a 0.25 mm sieve (60 mesh) prior to further analyses. Samples are hereafter referred to as WX00 (wood) and GX00 (grass) with "X" indicating the final charring temperature (100-700˚C). For comparison, fresh plant material (W000 and G000) was included in some analyses.

Characterization. All chars were subjected to the following procedures. Gravimetric analyses were conducted according to the American Society for Testing and Materials (ASTM) D1762-84 (*17*) to determine volatile matter, fixed C, and ash contents. Total carbon, nitrogen, and hydrogen were measured on a Carlo Erba NA-1500 CNS analyzer (Carlo Erba Instruments, Milan, Italy). BET-N_2 SA's of all char samples were obtained using an NOVA 2200e surface

area analyzer (Quantachrome Instruments Corp., Boynton Beach, FL). All N_2 measurements were performed in triplicate (N = 3). FT-IR spectroscopy was performed using a Thermo Nicolet Nexus 470 FT-IR 6700 spectrophotometer equipped with a smart endurance single-bounce diamond ATR accessory (Thermo Fisher Scientific, Waltham, MA). Diffraction patterns were recorded on a PANanalytical X'Pert Pro Instrument using Co-Kα radiation. Near-edge X-ray absorption fine structure spectra were collected using a synchrotron-based scanning transmission X-ray microscope (STXM) at the Advanced Light Source, Lawrence Berkeley National Laboratory, Beamline 5.3.2. A more detailed account of the production and characterization procedures and peak assignments for FT-IR and NEXAFS (Table S-1 and S-2, respectively) including references is available in the Supporting Information (SI).

Results and Discussion

Characterization. Table 1 displays the numerical results for proximate and elemental analyses and BET-N_2 SA measurements for wood and grass char samples generated at various charring temperatures. Yields begin to decline most rapidly at 200˚C for wood and at 300˚C for grass, and remain relatively stable above 400˚C. Final yields of grass char (~29%) are higher than those of wood char (~22%).

Volatile matter (VM) and fixed C contents gives a relative measure of the more labile and more stable components of chars, respectively (see SI for details). Volatile components of both wood and grass char decrease substantially between 400 and 600˚C. Fixed C values show a reverse trend in this temperature range. This corroborates observations by Schenkel (*18*) summarized in Antal and Gronli (*19*), who find a large increase of fixed C contents between 300 and 500˚C. Ash contents in wood char increase slightly at 400˚C and stabilize at ~4% at higher temperatures, whereas those of grass chars are generally higher and eventually stabilize at ~19%.

Relative elemental contents show the rapid loss of oxygen and hydrogen between 300 and 500˚C suggesting similar condensation reactions for wood and grass. When plotted in a typical van Krevelen diagram (as shown in the SI, Figure S-1), the progressive decrease in the H/C and O/C atomic ratios with temperature follows the trajectory associated with dehydration reactions (*20*). N contents are relatively stable for wood chars but show a maximum (1.24%) at 400˚C, indicating the enrichment of N-containing compounds. Starting at 400 and 500˚C for wood and grass chars, respectively, a dramatic rise in SA is observed with increasing temperatures. Final values for wood char (347 m^2 g^{-1}) are significantly higher than those of grass char (140 m^2 g^{-1}). The falloff in SA observed for wood chars at the final temperatures is consistent with observations showing SA maxima at relatively high temperatures (500-900˚C) (*19*).

FT-IR. The evolution of FT-IR spectra of wood and grass chars as a function of charring temperature is shown in Fig. 1. The reader is referred to the SI for a more detailed discussion of these results. To summarize, (i) no FT-IR detectable chemical changes occur as plant material is heated to 100 and 200˚C. Spectra then show (ii) dehydration of cellulosic and ligneous components starting at 300˚C (3500-3200 cm^{-1}), (iii) presence lignin/cellulose-derived transformation products at 400˚C (multiple peaks 1600-700 cm^{-1}), and (iv) an increasing degree of condensation at charring temperatures of 500˚C and beyond (loss of intensity at 1650-1500 cm^{-1} relative to 885-752 cm^{-1}).

XRD. The X-ray diffraction patterns of the grass and wood chars are represented in Fig. 2, showing intensity of the diffracted beam as a function of the Bragg angle (˚2θ). Sharp, non-labeled peaks in grass chars indicate miscellaneous inorganic components. Although not discussed in detail, the greater prevalence of these peaks is consistent with the higher percentage

of ash in the grass chars. Peak spacings of 0.60; 0.53; 0.404 and 0.259 nm are assigned to the hkl *101*, *110*, *200*, and *004* crystallographic planes of completely ordered (i.e., crystalline) regions of cellulose, respectively, assuming a monoclinic unit cell with c as the fiber axis (*21*). Spacings between 0.392 and 0.372 nm and between 0.209 and 0.207 nm are assigned to the hkl *002* and the overlapping *101*;*100* planes, respectively, of graphene sheets within turbostratic carbon crystallites (*14, 15*).

As the charring temperature increases from 100 to 300˚C, strong peaks from cellulose (i.e., 0.60, 0.53, 0.404, and 0.259 nm) progressively loose intensity and become broader (Fig. 2), indicating a gradual decrease in cellulose crystallinity. A complete loss of crystal structure in cellulose is indicated by the disappearance of the 0.60 and 0.53 nm signals and the coincidental shift of the 0.404 nm signal to higher angles in the 400˚C treatment (0.392 nm).

Further heating gives rise to broad peaks around 0.381 and 0.207 nm. The narrowing of these peaks with increasing temperature indicates developing atomic order in the increasingly carbonized plant material and is attributed to the formation and evolution of turbostratic crystallites. At advanced carbonization stages (i.e., temperatures > 400˚C), X-ray scattering has revealed progressive stacking of graphene sheets (*14, 16*). These small graphene packets are arranged in turbostratic disorder and therefore referred to as turbostratic crystallites. Lateral growth of graphene planes is indicated by the increasing intensity of the *101*;*100* planes at 0.208-0.207 nm (*22*). Note that the 0.381 nm peak in the wood chars is narrower and shows much higher intensities than the signal in the respective grass chars (Fig. 2), indicating that wood chars are significantly more crystalline. Compared to XRD peaks of pure graphite (*23*), those of G700 and W700 are broad and featureless. The presented results are a further indication of the

structural differences between chars consisting of turbostratic chrystallites and highly ordered graphite.

The XRD-data demonstrate that cellulose crystallinity of wood and grass chars is lost between 300 and 400˚C, while turbostratic crystallites evolve at charring temperatures above 400˚C. In addition to these two crystalline phases, X-ray scattering has revealed an intermediate, amorphous C stage within the narrow temperature interval 410-450˚C during the charring process of wood (*16*). Our data suggest such a disintegrated and entirely random C phase for wood and grass within a narrow temperature interval between 300 and 400˚C, where crystallinity stemming from both cellulosic components and turbostratic crystallites is at its minimum.

NEXAFS. Stacked C 1s NEXAFS spectra of each wood and grass char are displayed in Fig. 3. The large number of peaks observed at low temperatures (100-300˚C) demonstrates how the greater variety of C forms present in fresh plant material remains preserved. The 1s-π^* C=C transition at 285.3 eV corresponding to H-, CH_3- or C-bonded aromatic C (*24*) is more prominent for wood than for grass, which can be ascribed to the higher lignin content of woody material. Further, lignin in coniferous wood (here Ponderosa Pine) is comprised of phenolic monomers derived from coniferyl alcohol, forming a peak at 287 eV which is prominent in the wood spectra (*25*). However, we also expect a contribution of the mixed 1s-3p/σ^* resonance at this energy that correlates with aliphatic C-H. A second common feature associated with aromatic C is a broader band between 292 and 295 eV (1s-σ^* resonance) (*26*). Spectra of grass chars show additional features in the intermediate region (286-287.5 eV). Here resonances of carbonyl groups (286.4 eV), aliphatic C-H and phenolic C-OH (287.1-287.3 eV) are located. At higher energies, carboxyl C-OOH (288.6 eV) and C-O (289.3 eV) of (hemi)cellulose and lignin are found (see peak assignments in Table S-2).

With intensity gains for the prominent bands in wood (285 and 287 eV) and almost all characteristic peaks in grass char at 300˚C, spectral features appear to be in a transitional state toward those observed at higher temperatures.

Charring at 400˚C results in a pronounced increase in aromatic C (1s-π* transition at 285 eV) and a drastic loss of other functional groups. The 1s-π* transition band slightly broadens, extending towards 284-285 and 286 eV. Absorption bands at this energy correspond to C=C π-transitions of molecules with low energy π* states such as quinone-like components (*27, 28*). Concomitantly, almost all bands associated with O-containing and aliphatic groups in the intermediate region are lost.

Increasing the charring temperature leads to the formation of a plateau between 286 and 288 eV. The gradual increase of the ratio of absorption at 285 eV (aromatic C) to that at 286-288 eV (aliphatic/oxygen-containing C) is an indication of the increasingly condensed nature of these chars. In pure graphite samples, this plateau is found at a 285 to 286-288 eV ratio of ~2.0 (*29*). In our work, the ratio for wood and grass chars are ~1.0 at 400˚C and, as the plateau gradually flattens, rises to ~1.5 at 700˚C. The remaining absorbance at 286.4 eV and 288.6 eV may be due to residual oxygenated functional groups (*30, 31*). However, this region has also been associated with "interlayer states" caused by poor alignment of graphene sheets (*29, 32*).

The notion that condensation takes place is further supported by the broad absorption band emerging at 500˚C between 291 and 295 eV. This signal is thought to arise from 1s-σ* C=C transitions (*33*) and has a possible contribution of the 1s-σ* exciton band (see below). The 1s-π* transitions at 285 eV are characteristic of aromatic double bonds, but lack information on the degree of condensation of these aromatic components. The 1s-σ* resonance, however, has been used to infer the degree of condensation and the long-range order of other carbonaceous

materials (*28*, *34*). Sharp 1s-σ* exciton peaks absorbing between 291 and 292 eV (see Fig. 3 for an idealized peak representation insert) are induced by long-range ordering of extensive polycondensed domains (see the SI for a brief discussion of 1s-σ* excitons). We observe evidence for such distinct features in spectra of chars produced at 600 and 700˚C (Fig. 3). Brandes et al. (*29*) used 1s-π* transitions in combination with 1s-σ* resonance and exciton features to propose a scheme to classify the crystallinity (i.e., the degree of structural order) of natural graphite samples. According to this scheme, well-ordered graphite features both distinct peaks at 285 eV and 292 eV as well as a distinctive 1s-σ* exciton peak. A missing or poorly expressed exciton peak, however, is thought to indicate the presence of smaller graphene sheets. Chars produced at 600 and 700˚C in this study would fall in the latter category, thus representing poorly crystalline materials.

NEXAFS spectra for chars reveal that (i) aromatic and quinonic compounds become prevalent while O-containing and aliphatic groups are lost at 400˚C, (ii) first evidence for condensation reactions is found at 500˚C, and (iii) chars produced at 600 and 700˚C are poorly crystalline in nature.

Specific Char Categories and their Components. FT-IR, XRD, and NEXAXS illustrate how chars derived from wood and grass biomass experience several phase transitions leading from microcrystalline cellulose over a largely amorphous intermediate phase towards the formation of turbostratic crystallites. They allow for the identification of four distinct categories of char (Figure 4).

Plant material - largely unaltered by thermal treatment

At initial charring stages, char yield and XRD-data indicate the loss of water and initial dehydration reactions of the wood and grass precursors. Overall, the native structure of the plant biopolymers (i.e., cellulose, hemicellulose, and lignin) remains preserved.

Transition chars - volatile dissociation products forming amorphous centers amidst a largely intact crystalline matrix

At the next charring stage, FT-IR spectra (loss of 1030 cm^{-1} peak) and lower H/C and O/C ratio clearly show that plant materials increasingly undergo dehydration and depolymerization of plant biopolymers, creating small volatile dissociation products. Greater signals of ketones, aldehyde, and carboxyl C observed in FT-IR spectra are indicative of depolymerization products derived from lignin (*35*) and cellulose (*36*). Volatile compounds such as anhydrosugars, pyrans, and furans are typical transformation products (*37-39*). Moreover, the stronger presence of phenols (NEXAFS absorbance at 285 eV and 287 eV) may form through secondary reactions of cellulose-derived intermediates (*38*). Despite the dissociation of such products, lignin sustains strong IR absorption (at 1510, 1440, and 1375 cm^{-1}) and XRD patterns illustrate that cellulose retains a notable portion of its crystallinity.

Amorphous char - an entirely amorphous mixture comprised of small, heat-resistant aliphatic and (hetero)aromatic elements

The sharp rise in aromatic C detected spectroscopically and the increasing growth of XRD reflections associated with condensation reactions are characteristic of this charring stage. The absence of pronounced 1s-σ* features in the NEXAFS data indicates that there is not yet significant long range ordering as expected in the presence of larger condensed sheets. Instead, broad XRD signals present at 0.392-0.372 and 0.209-0.207 nm suggest the dominance of small aromatic units arranged in random order. In good agreement with the model proposed by

Knicker et al. (*12, 13*) and studies of pyrolysis processes (*19, 37-39*), we observe (i) the formation of intermediates such as pyranones, anhydrosugars, phenols, quinones, pyrroles, and furans as well as small (poly)aromatic units, and (ii) the relative enrichment of stable aromatic lignin residues due to the loss of less heat-resistant material reflected in the dramatic decline in char yield, non-C atoms, and VM contents. In addition, substantial amounts of VM, along with aliphatic signals in NEXAFS and FT-IR spectra, suggest that not only cyclic and aromatic volatiles are retained. Almendros et al. (*40*) proposed that aliphatic components such as cutans and lipids are "fixed" in predominantly aromatic matrices, thereby resisting volatilization and degradation. The fact that crystalline cellulose is almost completely depolymerized combined with the evidence presented above suggest a disintegrated and randomly disordered C phase.

Composite char - turbostratic crystallites embedded in a low-density amorphous phase

A larger degree of condensation as reflected in FT-IR (out-of-plane vibrations) and NEXAFS spectra (285 to 286-288 eV ratio) and the formation of turbostratic crystallites as seen in the *002* XRD reflections are distinctive for chars formed upon further heating.

BET-N_2 SA values are well below the maximum achieved at higher temperatures, while gravimetric and elemental analyses indicate that some volatile non-condensed components are retained in the char matrix. Bourke et al. (*23*) found that the lack of atomic pore space within the crystallite carbon layers as well as recondensation and trapping of VM in pores reduces the SA. Spectroscopic information presented in this study points specifically to the preservation of aromatic, aliphatic, and O-containing components, forming the amorphous matrix surrounding turbostratic crystallites.

Turbostratic char - nanoporous phase of turbostratic crystallites

At high temperatures, successive growth and increasing long-range order of the turbostratic crystallites are seen. Condensation proceeds as inferred from the more prominent 1s-σ* resonance band in NEXAFS spectra, whereas the appearance of the exciton feature, along with the evolution of the *002* XRD reflection, verifies the presence of increasingly crystalline structures. The dramatic rise in N_2-accessible SA at this charring stage is in part due to the lateral growth of graphene-like sheets at the expense of amorphous C (both aromatic and aliphatic) (*14*). The graphitic crystallites are denser than the original amorphous C forms, thus conversion of the former into the latter eventually leads to the formation of nanopores (d < 2 nm). Moreover, the fact that turbostratic chars are poorly crystalline in nature maintains a clear division between chars and natural or synthetic graphite. Bourke et al. (*23*) revealed the structural differences using XRD in conjunction with NMR and MALDI-TOF MS. It is shown that the relatively high heteroatom content, SA, electrical conductivity, and the abundance of unpaired electrons in the structure unequivocally distinguish chars from graphite.

Fig. 4B summarizes the trends in char and fixed-C yield observed herein as well as those discussed in the review by Antal and Gronli (*19*). Collectively these studies report a rapid decrease in char yield and a relative increase in fixed-C yield at charring temperatures greater than ~250-300˚C followed by a stabilization in yields at charring temperatures greater than ~700˚C.

Comparison of Precursor Materials. FT-IR spectra and elemental ratios suggest that the breakdown of grass appears to begin at slightly lower temperatures than that of wood. Generally, heat-induced decomposition of hemicellulose and cellulose in biomass occurs rapidly at low temperatures (between 230-400˚C), whereas that of lignin happens over a broader temperature range (160-900˚C) (*41*). This suggests that the activation energy for heat-induced

alteration of grass char is lower, presumably due to higher contents of thermally labile hemicelluloses, than for the more complex ligneous polymer structure of wood. The relative quantities of biopolymers in the native plant material thus determine the specific conditions under which biomass charring yields transition chars (Fig. 4).

The transition from amorphous C into ordered turbostratic crystallites is not only seen for wood chars, but also quite evident for grass chars. Consequently, the two-phase model by Kercher and Nagle (*14*) initially developed for wood chars may be applicable to various types of plant biomass. However, it is clear that higher yields of crystalline chars with larger SAs from wood can be achieved at lower temperatures than from grass biomass. This will be important for applications seeking to maximize the reactivity of chars as soil amendments (*5*).

Implications for degradability are probable and already have been suggested. Hamer et al. (*42*) showed that corn stover and rye char were mineralized more rapidly than wood char. Nguyen and Lehmann (*43*) reported that mineralization and oxidation decrease at higher temperatures for corn (grass) chars, whereas no such effect was observed for oak (wood) char.

Environmental Implications

Persistence in the Environment. The "paradox of refractory-labile BC" (*44*) refers to the lack of explanations for the large observed differences in residence time between seemingly refractory BC forms and other forms that appear to be more dynamic. Our investigation has revealed structural and chemical differences which make it plain that the persistence of BC in the environment depends to a great extend on its particular chemistry and physical structure. Attempts to rationalize observed variations in the chars' resistance to abiotic and biotic degradation (or "aging") (*20, 42*) will lead to more robust results when they are based on the multiphase model presented in Figure 4.

Chars as Environmental Sorbents. A clear distinction between the categories of chars and their various phases entering soils and sediments will aid the more accurate description of the sorption behavior of organic contaminants. Different types of char have different BC-water distribution coefficients (K_{BC}) values (*2*). These variations are attributed to differences in SA and pore size distributions which are well-reflected in the proposed categories. Chen et al. (*10*) divides chars into a non-condensed partition (absorption) medium and carbonized phases that are viewed as a sorbent surface, but are indifferent toward the molecular properties of the non-condensed phase. Our results show that mobile, non-condensed components may comprise both crystalline (i.e., native cellulose) and heat-altered amorphous components (i.e., lignin residues, aliphatics, and small (poly)aromatic units) which are expected to show dissimilar sorptive behavior.

Quantification in Environmental Systems. Despite substantial progress, different techniques yield widely varying BC "contents" for soils and sediments (*9*). These authors conclude that all quantification methods are selective, e.g., for amorphous wood char or more condensed wood chars. We suggest considering that the quantification protocols tested might be selective for one or more char categories. The reader is referred to the SI for a more detailed account of the environmental implications of the structural differences among the char categories.

We conclude with the suggestion that future research efforts need to recognize the existence of various categories of char BC with distinct (i) physical architecture and (ii) molecular compositions (Fig. 4). The unique combination of physical and chemical features in each category is likely to translate into widely differing dynamics and functions in soil and sediment environments. Future investigations of the effect of both charring conditions (e.g.,

charring duration and ramp rates) and biomass properties (e.g., other than wood and grass) on properties and yields of individual char categories will help to refine the presented classification scheme.

Acknowledgements

We thank F. Prahl and M. Sparrow for assistance with pyrolysis procedures and elemental analysis, and D. Kilcoyne for providing "after hours" support at ALS beamline 5.3.2. M. Keiluweit acknowledges a merit scholarship awarded by the Department of Crop and Soil Science (OSU).

Partial support was provided by the Office of Science, Climate and Environmental Science Division, of the U.S. DOE under Contract DE-AC02-05CH11231. Use of the ALS was provided by U.S. DOE, Office of Science, Basic Energy Sciences under the same contract. The information in this document has been funded in part by the U.S. Environmental Protection Agency. It has been subjected to review by the National Health and Environmental Effects Research Laboratory's Western Ecology Division and approved for publication. Approval does not signify that the contents reflect the views of the agency, nor does mention of trade names or commercial products constitute endorsement or recommendation for use.

Supporting Information Available

Additional information includes detailed descriptions of char production and FT-IR procedures; FT-IR and NEXAFS peak assignments; the van Krevelen plot of char elemental contents; discussion of the 1s-σ* exciton phenomenon (NEXAFS); and a more detailed account of environmental implications of the proposed char categories.

Literature Cited

(1) Kuhlbusch, T. A. J., Black carbon and the carbon cycle. *Science* **1996,** 280, 1903-1904.

(2) Koelmans, A. A.; Jonker, M. T. O.; Cornelissen, G.; Bucheli, T. D.; Van Noort, P. C. M.; Gustafsson, O., Black carbon: The reverse of its dark side. *Chemosphere* **2006,** 63(3), 365-377.

(3) Masiello, C. A., New directions in black carbon organic geochemistry. *Mar. Chem.* **2004,** 92(1-4), 201-213.

(4) Preston, C. M.; Schmidt, M. W. I., Black (pyrogenic) carbon: a synthesis of current knowledge and uncertainties with special consideration of boreal regions. *Biogeosciences* **2006,** 3(4), 397-420.

(5) Lehmann, J., Bio-energy in the black. *Front Ecol Environ* **2007,** 5(7), 381-387.

(6) Lehmann, J., A handful of carbon. *Nature* **2007,** 447(7141), 143-144.

(7) Loganathan, V. A.; Feng, Y.; Sheng, G. D.; Clement, T. P., Crop-residue-derived char influences sorption, desorption and bioavailability of atrazine in soils. *Soil Sci. Soc. Am. J.* **2009,** 73, 967-974.

(8) Seiler, W.; Crutzen, P. J., Estimates of gross and net fluxes of carbon between the biosphere and the atmosphere from biomass burning. *Climatic Change* **1980,** 2, 207-247.

(9) Hammes, K.; Schmidt, M. W. I.; Smernik, R. J.; Currie, L. A.; Ball, W. P.; Nguyen, T. H.; Louchouarn, P.; Houel, S.; Gustafsson, Ö.; Elmquist, M., et al. Comparison of quantification methods to measure fire-derived (black/elemental) carbon in soils and sediments using reference materials from soil, water, sediment and the atmosphere. *Global Biogeochem. Cycles* **2007,** 21(3), GB3016, doi:10.1029/2006GB002914.

(10) Chen, B.; Zhou, D.; Zhu, L., Transitional adsorption and partition of nonpolar and polar aromatic contaminants by biochars of pine needles with different pyrolytic temperatures. *Environ. Sci. Technol.* **2008,** 42(14), 5137-5143.

(11) Hedges, J. I.; Eglinton, G.; Hatcher, P. G.; Kirchman, D. L.; Arnosti, C.; Derenne, S.; Evershed, R. P.; Kogel-Knabner, I.; de Leeuw, J. W.; Littke, R.; Michaelis, W.; Rullkotter, J., The molecularly-uncharacterized component of nonliving organic matter in natural environments. *Org. Geochem.* **2000,** 31(10), 945-958.

(12) Knicker, H., How does fire affect the nature and stability of soil organic nitrogen and carbon? A review. *Biogeochemistry* **2007,** 85(1), 91-118.

(13) Knicker, H.; Hilscher, A.; Gonzalez-Vila, F. J.; Almendros, G., A new conceptual model for the structural properties of char produced during vegetation fires. *Org. Geochem.* **2008,** 39(8), 935-939.

(14) Kercher, A. K.; Nagle, D. C., Microstructural evolution during charcoal carbonization by X-ray diffraction analysis. *Carbon* **2003,** 41(1), 15-27.

(15) Kumar, M.; Gupta, R. C.; Sharma, T., X-ray diffraction studies of Acadia and Eucalyptus wood chars. *J. Mater. Sci.* **1993,** 28, 805-810.

(16) Paris, O.; Zollfrank, C.; Zickler, G. A., Decomposition and carbonisation of wood biopolymers - a microstructural study of softwood pyrolysis. *Carbon* **2005,** 43(1), 53-66.

(17) ASTM, *D1762-84 Standard Test Method for Chemical Analysis of Wood Charcoal*. Conshohocken, PA, 2007.

(18) Schenkel, Y. Modelisation des flux massiques et energetiques dans la carbonisation du bois en four Cornue. Ph.D. Dissertation, Gembloux, Belgium, 1999.

(19) Antal, M.; Gronli, M., The art, science, and technology of charcoal production. *Ind. Eng. Chem. Res.* **2003,** 42(8), 1619-1640.

(20) Baldock, J. A.; Smernik, R. J., Chemical composition and bioavailability of thermally altered Pinus resinosa (Red Pine) wood. *Org. Geochem.* **2002,** 33(9), 1093-1109.

(21) Koyama, M.; Helbert, W.; Imai, T.; Sugiyama, J.; Henrissat, B., Parallel-up structure evidences the molecular directionality during biosynthesis of bacterial cellulose. *Proc. Natl. Acad. Sci. U. S. A.* **1997,** 94(17), 9091-9095.

(22) Byrne, C.; Nagle, D., Carbonized wood monoliths - Characterization. *Carbon* **1997,** 35(2), 267-273.

(23) Bourke, J.; Manley-Harris, M.; Fushimi, C.; Dowaki, K.; Nunoura, T.; Antal, M. J., Do all carbonized charcoals have the same chemical structure? 2. A model of the chemical structure of carbonized charcoal. *Ind. Eng. Chem. Res.* **2007,** 46(18), 5954-5967.

(24) Urquhart, S. G.; Ade, H.; Rafailovich, M.; Sokolov, J. S.; Zhang, Y., Chemical and vibronic effects in the high-resolution near-edge X-ray absorption fine structure spectra of polystyrene isotopomers. *Chem. Phys. Lett.* **2000,** 322(5), 412-418.

(25) Cody, G.; Brandes, J.; Jacobsen, C.; Wirick, S., Soft X-ray induced chemical modification of polysaccharides in vascular plant cell walls. *J. Electron Spectrosc. Relat. Phenom.* **2009,** 170(1-3), 57-64.

(26) Cody, G.; Botto, R.; Ade, H.; Behal, S.; Disko, M.; al., e., Inner-shell spectroscopy and imaging of a subbituminous coal: In-situ analysis of organic and inorganic microstructure using C (1s)-, Ca (2p)-, and Cl (2s)-NEXAFS. *Energy Fuels* **1995,** 9, 525-533.

(27) Francis, J. T.; Hitchcock, A. P., Inner-shell spectroscopy of para-benzoquinone, hydroquinone, and phenol - distinguishing quinoid and benzenoid structures. *J. Phys. Chem.* **1992,** 96(16), 6598-6610.

(28) di Stasio, S.; Braun, A., Comparative NEXAFS study on soot obtained from an ethylene/air flame, a diesel engine, and graphite. *Energy Fuels* **2006,** 20(1), 187-194.

(29) Brandes, J. A.; Cody, G. D.; Rumble, D.; Haberstroh, P.; Wirick, S.; Gelinas, Y., Carbon K-edge XANES spectromicroscopy of natural graphite. *Carbon* **2008,** 46(11), 1424-1434.

(30) Cody, G. D.; Ade, H.; Wirick, S.; Mitchell, G. D.; Davis, A., Determination of chemical-structural changes in vitrinite accompanying luminescence alteration using C-NEXAFS analysis. *Org. Geochem.* **1998,** 28(7-8), 441-455.

(31) Hitchcock, A. P.; Urquhart, S. G.; Rightor, E. G., Inner-shell spectroscopy of benzaldehyde, terephthaladehyde, ethyl benzoate, terephthaloyl chloride, and phosgene - models for core excitation for poly(ethylene-terephthalate). *J. Phys. Chem.* **1992,** 96(22), 8736-8750.

(32) Fischer, D. A.; Wentzcovitch, R. M.; Carr, R. G.; Continenza, A.; Freeman, A. J., Graphitic interlayer states – a carbon-K near-edge X-ray-absorption fine-structure study. *Phys. Rev. B: Condens. Matter* **1991,** 44(3), 1427–1429.

(33) Stöhr, J., *NEXAFS spectroscopy*. Springer: New York, 1996.

(34) Banerjee, S.; Hemraj-Benny, T.; Balasubramanian, M.; Fischer, D. A.; Misewich, J. A.; Wong, S. S., Surface chemistry and structure of purified, ozonized, multiwalled carbon nanotubes probed by NEXAFS and vibrational spectroscopies. *ChemPhysChem* **2004,** 5(9), 1416-1422.

(35) Liu, Q.; Wang, S.; Zheng, Y.; Luo, Z.; Cen, K., Mechanism study of wood lignin pyrolysis by using TG-FTIR analysis. *J. Anal. Appl. Pyrolysis* **2008,** 82(1), 170-177.

(36) Reeves, J. B.; McCarty, G. W.; Rutherford, D. W.; Wershaw, R. L., Mid-infrared diffuse reflectance spectroscopic examination of charred pine wood, bark, cellulose, and lignin: Implications for the quantitative determination of charcoal in soils. *Appl. Spectrosc.* **2008,** 62(2), 182-189.

(37) Essig, M. G.; Richards, G. N.; Schenck, E. M., Mechanisms of formation of the major volatile products from the pyrolysis of cellulose. In *Cellulose and Wood Chemistry and Technology*, Schuerch, C., Ed. J. Wiley & Sons: New York, 1989.

(38) Pastorova, I.; Botto, R. E.; Arisz, P.; Boon, J., Cellulose char structure - a combined analytical PY-GC-MS, FTIR, and NMR-study. *Carbohydr. Res.* **1994,** 262(1), 27-47.

(39) Shafizadeh, F., Introduction to pyrolysis of biomass. *J. Anal. Appl. Pyrolysis* **1982,** 3(4), 283-305.

(40) Almendros, G.; Knicker, H.; Gonzalez-Vila, F. J., Rearrangement of carbon and nitrogen forms in peat after progressive thermal oxidation as determined by solid-state C-13 and N-15-NMR spectroscopy. *Org. Geochem.* **2003,** 34(11), 1559-1568.

(41) Yang, H.; Yan, R.; Chen, H.; Lee, D. H.; Zheng, C., Characteristics of hemicellulose, cellulose and lignin pyrolysis. *Fuel* **2007,** 86(12-13), 1781-1788

(42) Hamer, U.; Marschner, B.; Brodowski, S.; Amelung, W., Interactive priming of black carbon and glucose mineralisation. *Org. Geochem.* **2004,** 35(7), 823-830.

(43) Nguyen, B. T.; Lehmann, J., Black carbon decomposition under varying water regimes. *Org. Geochem.* **2009,** 40(8), 846-853.

(44) Czimczik, C. I.; Masiello, C. A., Controls on black carbon storage in soils. *Global Biogeochem. Cycles* **2007,** 21(3), GB3005, doi:10.1029/2006GB002798.

TABLE 1. Char and fixed-C yields, volatile matter, and ash contents, elemental composition and ratios, and BET-N_2 surface area (N=3) of wood and grass chars prepared at various charring temperatures.

Sample	Yield	VM	Fixed C	Ash	C	N	H	O	H/C	O/C	BET-N_2 SA[a]
	[wt %][b]								atomic ratio[b]		[m^2 g^{-1}]
W100	99.8	77.1	21.7	1.2	50.6	0.05	6.68	42.7	1.59	0.63	1.6±0.3
W200	95.9	77.1	21.4	1.5	50.9	0.04	6.95	42.2	1.64	0.62	2.3±0.1
W300	62.2	70.3	28.2	1.5	54.8	0.05	6.50	38.7	1.42	0.53	3.0±0.0
W400	35.3	36.4	62.2	1.4	74.1	0.06	4.95	20.9	0.80	0.21	28.7±1.5
W500	28.4	25.2	72.7	2.1	81.9	0.08	3.54	14.5	0.52	0.13	196±11
W600	23.9	11.1	85.2	3.7	89.0	0.06	2.99	8.0	0.40	0.07	392±11
W700	22.0	6.3	92.0	1.7	92.3	0.08	1.62	6.0	0.21	0.05	347±11
G100	99.9	69.6	23.5	6.9	48.6	0.64	7.25	44.1	1.81	0.69	1.8±0.4
G200	96.9	70.7	23.6	5.7	47.2	0.61	7.11	45.1	1.81	0.72	3.3±0.4
G300	75.8	54.4	36.2	9.4	59.7	1.02	6.64	32.7	1.34	0.41	4.5±0.6
G400	37.2	26.8	56.9	16.3	77.3	1.24	4.70	16.7	0.73	0.16	8.7±0.5
G500	31.4	20.3	64.3	15.4	82.2	1.09	3.32	13.4	0.48	0.12	50±0.4
G600	29.8	13.5	67.6	18.9	89.0	0.99	2.47	7.6	0.33	0.06	75±12
G700	28.8	9.1	71.6	19.3	94.2	0.70	1.53	3.6	0.20	0.03	139±11

[a] Shown are average values calculated from N replicate measurements ± standard deviations.

[b] Yields and fixed C, ash, and VM contents are on a water-free basis (dried at 105˚C). Elemental contents and atomic ratios are on water- and ash-free basis.

Figure captions

Figure 1: Stacked ATR FT-IR spectra of (a) wood and (b) grass char samples heated to temperatures ranging from 100 to 700˚C.

Figure 2: X-ray diffraction profiles (cobalt radiation) of (a) wood and (b) grass chars generated at temperatures ranging from 100 to 700˚C. Vertical lines indicate peak positions; associated numbers are d-spacings between crystallographic planes in nm. Sharp, non-labeled peaks are from inorganic components.

Figure 3: C NEXAFS spectra of (a) wood and (b) grass char temperature series including a non-charred sample of each. Individual spectra are shifted on the absorbance axis for better discrimination. The grey shaded area indicates the region in which 1s-σ* resonance and 1s-σ* exciton peak are located. The black line represents the idealized spectral features arising from 1s-σ* exciton and resonance characteristic of highly conjugated graphene sheets adapted from Brandes et al. (*29*). Additionally, absorption bands at 297.2 and 299 eV are attributed to potassium (K) L_{III} and L_{II} edges, respectively.

Figure 4: Dynamic molecular structure of plant biomass-derived black carbon (biochar) across a charring gradient and schematic representation of the four proposed char categories and their individual phases. (A) Physical and chemical characteristics of organic phases. Exact temperature ranges for each category are controlled by both charring conditions (i.e., temperature, duration, and atmosphere) and relative contents of plant biomass components (i.e., hemicellulose, cellulose, and lignin). (B) Char composition as inferred from gravimetric analysis. Yields, VM, fixed-C, and ash contents are averaged across wood and grass chars. Relative contributions above 700˚C are estimates.

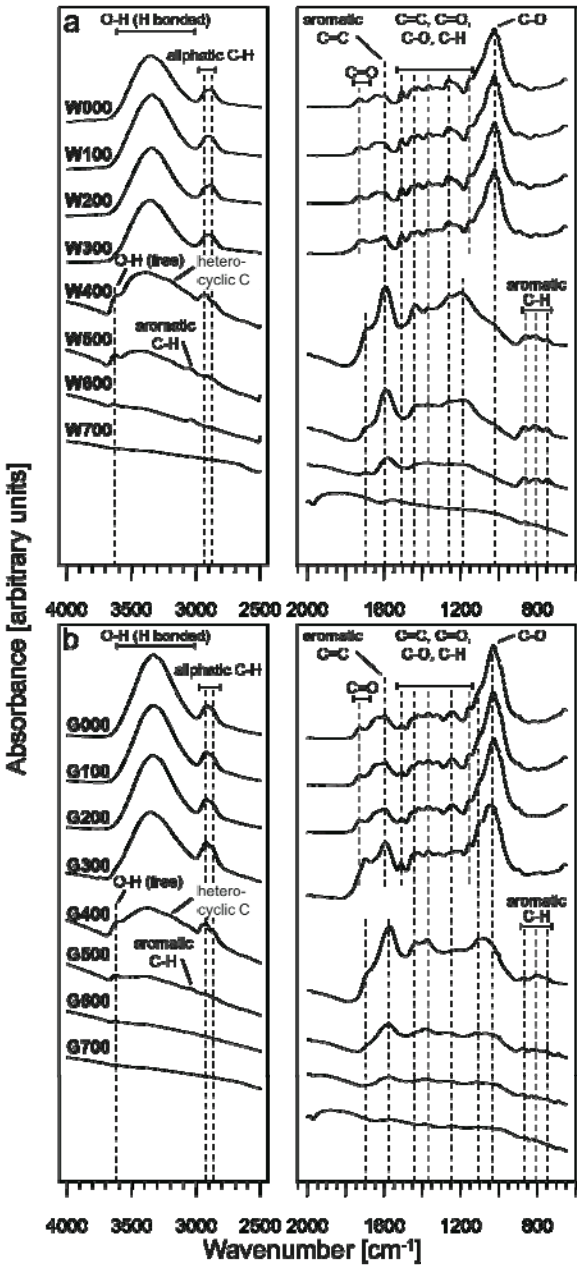
a
O-H (H bonded)
aliphatic C-H
W000
W100
W200
W300
O-H (free)
hetero-
cyclic C
W400
aromatic
C-H
W500
W600
W700
aromatic
C=C
C=C, C=O,
C-O, C-H
C-O
aromatic
C-H
b
G000
G100
G200
G300
G400
G500
G600
G700
Absorbance [arbitrary units]
4000 3500 3000 2500 2000 1600 1200 800
Wavenumber [cm-1]

Figure 1

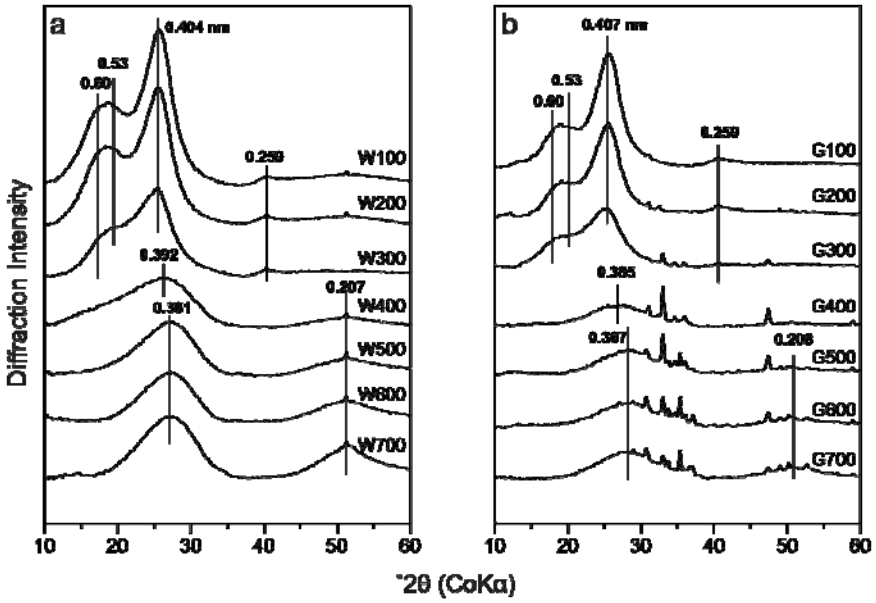
a
0.404 nm
0.53
0.80
0.259
W100
W200
W300
0.392
0.381
0.207
W400
W500
W600
W700
b
0.407 nm
0.53
0.80
0.259
G100
G200
G300
0.385
G400
0.387
0.208
G500
G600
G700
Diffraction Intensity
10
20
30
40
50
60
2θ (CoKα)

Figure 2

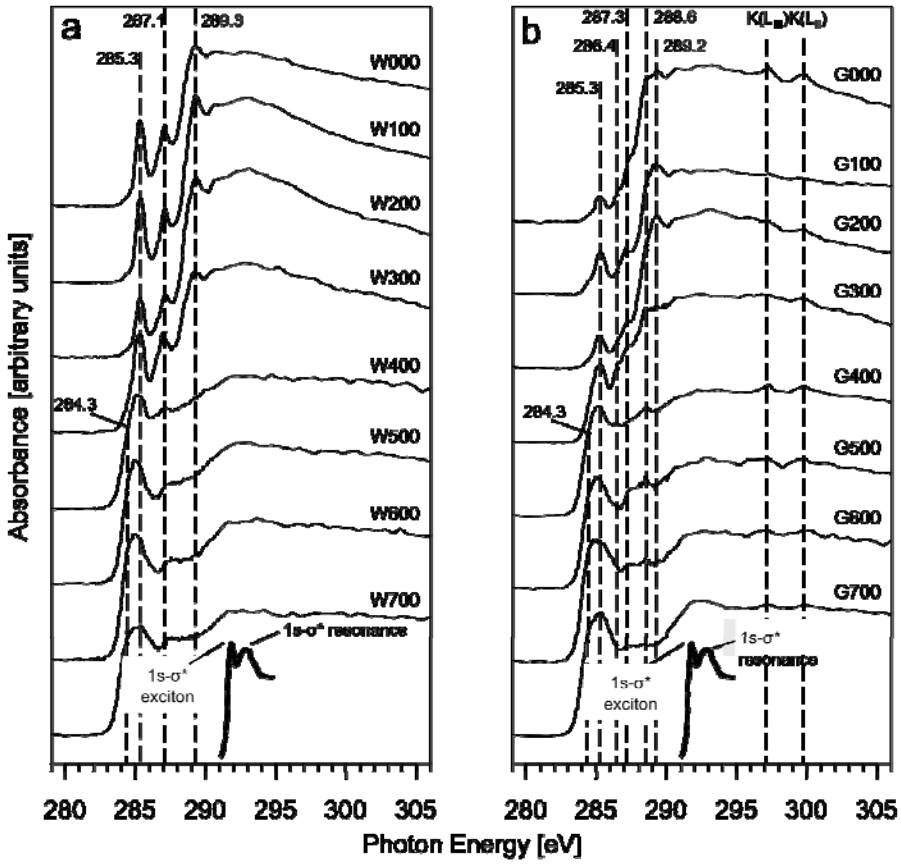
a
287.1
289.9
285.3
W000
W100
W200
W300
W400
284.3
W500
W600
W700
1s-σ* resonance
1s-σ*
exciton
b
287.3
288.6
K(L$_{III}$)K(L$_{II}$)
286.4
289.2
285.3
G000
G100
G200
G300
G400
284.3
G500
G600
G700
1s-σ*
resonance
1s-σ*
exciton
Absorbance [arbitrary units]
280
285
290
295
300
305
Photon Energy [eV]

Figure 3

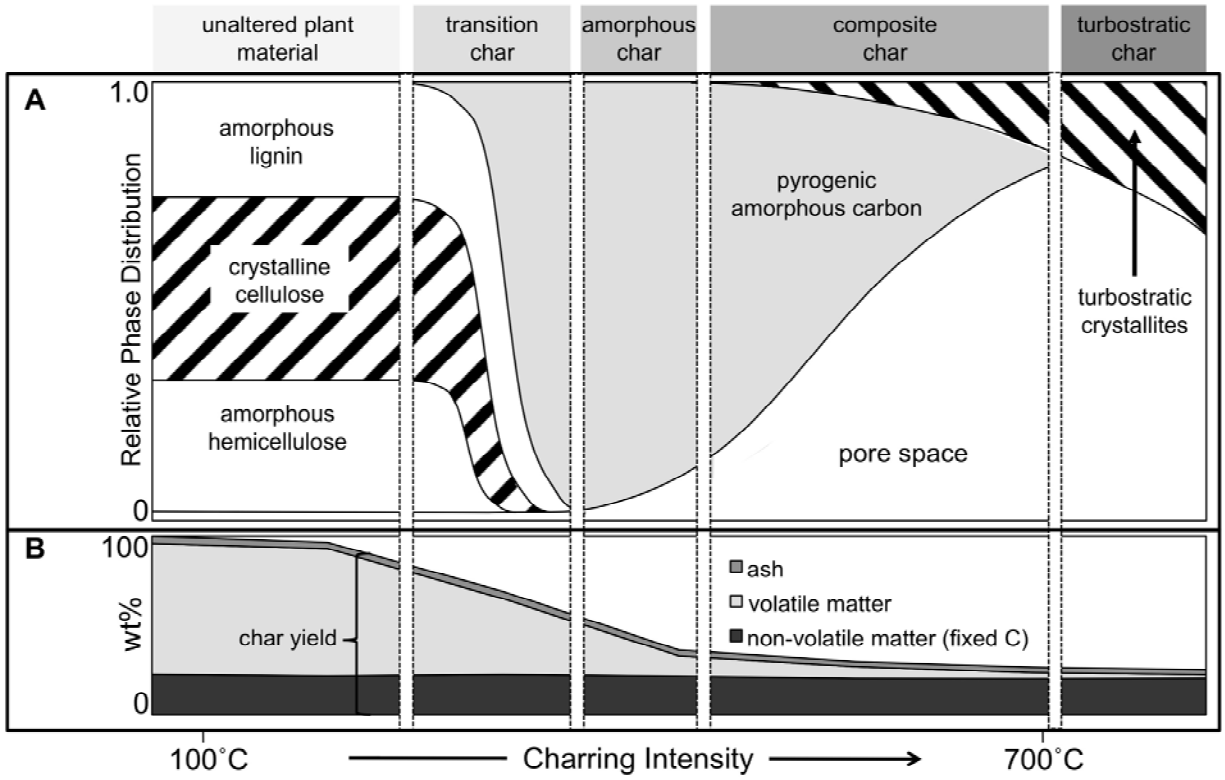
unaltered plant material
transition char
amorphous char
composite char
turbostratic char
A
1.0
Relative Phase Distribution
amorphous lignin
crystalline cellulose
amorphous hemicellulose
0
pyrogenic amorphous carbon
pore space
turbostratic crystallites
B
100
wt%
char yield
0
ash
volatile matter
non-volatile matter (fixed C)
100˚C
Charring Intensity
700˚C

Figure 4